JUNE 01 2006

Characterization of impedance boundary as damped harmonic oscillators via impulse reflection

K.-Y. Fung; Xiaodong Jing

J. Acoust. Soc. Am. 119, 3831–3838 (2006)
https://doi.org/10.1121/1.2198185

Characterization of impedance boundary as damped harmonic oscillators via impulse reflection

K.-Y. Fung[a] and Xiaodong Jing[b]
Department of Mechanical Engineering, The Hong Kong Polytechnic University, Hung Hom, Kowloon, Hong Kong, People's Republic of China

(Received 17 August 2005; revised 10 March 2006; accepted 26 March 2006)

This paper demonstrates that various sound-absorbing/reflective materials or structures can be effectively characterized over a wide band of frequency by the sum of only a few damped harmonic oscillators. This method is physically sound in the sense that each damped harmonic oscillator corresponds to the natural resonance of the impedance boundary as it is numerically advantageous to afford a simple, recursive, efficient, and unconditionally stable boundary algorithm for computational aero-acoustics applications. The time-domain damped-harmonic-oscillator impedance characterization method is finally validated by accurate predictions of reflected pulses from impedance boundaries physically formed of Helmholtz resonators or various exits of a circular pipe. © *2006 Acoustical Society of America.* [DOI: 10.1121/1.2198185]

PACS number(s): 43.58.Bh, 43.20.El, 43.20.Ye, 43.20.Bi [JBS] Pages: 3831–3838

I. INTRODUCTION

The problem of sound reflection is of fundamental importance to acoustics, and the concept of acoustic impedance $Z=\hat{p}/\hat{u}_n$, defined in the frequency domain by the ratio Fourier-transformed acoustic pressure $\hat{p}$ and velocity $\hat{u}_n$ normal into a surface, has led to numerous successful treatments and applications for noise control and abatement. The recent advances and interest in computational aero-acoustics (CAA) necessitate the extension of acoustic impedance to its time-domain equivalent for transient or broadband analysis. Various methods have been proposed for the construction of the time-domain equivalent of acoustic impedance and its efficient implementation as a general boundary condition.[1,2] These methods, however, have been indirectly inferred from data taken under the harmonic assumption. Moreover, with regard to the proper mathematical treatment of a boundary condition, little attention has been given to the physical implications of the equivalent time-domain reflection process of an impedance boundary. In this paper, a direct time-domain method of characterizing an impedance boundary is proposed which finds its basis on the resonance nature of practical sound-absorbing materials or structures.

When the classical concept of impedance is extended to its time-domain equivalent, the concern of causality arises. The direct inverse Fourier transform of a frequency-domain impedance model, such as the two- or three-parameter impedance models for porous materials, generally fails to give a causal time-domain impedance boundary condition (TDIBC), as discussed by Berthelot.[3] The reason is that an analytical, numerical, or empirical impedance model in the frequency domain is likely to have been constructed from a relation or data that are frequency band limited, and therefore is incapable of the provision of asymptotically correct behaviors.

Recently, Fung and Ju[4,5] proposed the construction of causal, stable TDIBC through the ratio of domain-exiting and entering characteristics and in the form of a system of damped harmonic oscillators, plausibly related to the physical resonance of a sound-absorbing material. Their method renders simple, recursive, efficient, and unconditionally stable TDIBC as a generalized closure for the linearized Euler's equation. Actually, in the field of electromagnetism, damped sinusoids identified from the transient response of a conducting object have long been treated as the "fingerprints" of the object and used for target identification.[6] This lends credence and support for finding its counterpart in acoustics.

Here, we systematically examine several well-used sound-absorbing structures or materials and present the results for micro-perforate panels (MPP), porous panels, Helmholtz-resonator structures, and various pipe exits. It is demonstrated that the physically realized, time-domain damped-harmonic-oscillator behavior of an impedance boundary is inherently related to the natural resonances of the sound-absorbing structure or material. From a physical point of view, there are three basic features within a physical impedance boundary: damping, mass, and elasticity. A simple combination of these features forms physically a damped harmonic oscillator (DHO) or mathematically a damped sinusoid. Complex impedance behaviors are simply the result of a combination of a series of damped harmonic oscillators. It is further shown that just a few of such oscillators can render a reflection coefficient model valid over a broad bandwidth of frequency for the commonly used sound-absorbing materials and structures. It is physically sound as it is numerically advantageous for their immediate applicability as TDIBC.

An impulse acoustic experiment is designed to validate the proposed time-domain impedance characterization

[a]Author to whom correspondence should be addressed. Electronic mail: mmkyfung@polyu.edu.hk
[b]Present address: School of Jet Propulsion, No. 407, Beijing University of Aeronautics and Astronautics, Beijing 100083, P. R. China. Electronic mail: jingxd@buaa.edu.cn

method. In the experiment, a short-duration acoustic pulse instead of a harmonic wave is used to examine the reflection property of a physical impedance boundary such as a Helmholtz-resonator terminus or exit in a one-dimensional waveguide. It is demonstrated that the measured reflected pulse can be accurately predicted by an acoustic propagation model based on the DHO characterization of the impedance boundary.

II. DHO AS ACOUSTIC BOUNDARY DESCRIPTOR

The reflectivity of an impedance boundary is conventionally characterized by the reflection coefficient $\hat{W}(\omega)$, which is generally a complex-valued function of real angular frequency ω defined by the ratio of the reflected sound pressure $\hat{p}^-(\omega)$ to the incident $\hat{p}^+(\omega)$,

$$\hat{W}(\omega) = \frac{\hat{p}^-(\omega)}{\hat{p}^+(\omega)}, \tag{1}$$

and is related to the acoustic impedance $Z(\omega)$ as

$$\hat{W}(\omega) = \frac{Z(\omega) - 1}{Z(\omega) + 1}. \tag{2}$$

On the assumption that $\hat{W}(\omega)$ can be analytically continued to the entire complex ω plane and that only causal reflection processes are physically realizable, i.e., $\int_{-\infty}^{0} p^+(t-\tau)W(\tau)d\tau = 0$, the poles of $\hat{W}(\omega)$ must lie in the upper half complex plane so the inverse Fourier transform of $\hat{W}(\omega)$ is

$$W(t) = jH(t)\sum_k \text{residues}[\hat{W}(\omega)e^{j\omega t}, \lambda_k], \tag{3}$$

where λ_k are the poles of $\hat{W}(\omega)$, $j=\sqrt{-1}$, and $H(t)$ is the Heaviside function. Thus, the time-domain equivalent of the reflection coefficient is the reflection impulse,

$$W(t) = A_0\delta(t) + H(t)\sum_k A_k \exp(j\lambda_k t) + A_k^* \exp(j\lambda_k^* t). \tag{4}$$

Here, λ_k are also referred as the complex natural frequencies, whose physical meaning will be discussed next, and A_k are correspondingly the complex amplitudes or residues. The δ function in Eq. (4) results from the limiting value of $\lim_{\omega\to\infty}|\hat{W}(\omega)|$. Since $W(t)$ must be real, both the natural frequencies and the complex amplitudes appear in pairs as $\lambda_k, \lambda_k^* = \pm\alpha_k + j\beta_k$ and $A_k, A_k^* = a_k \pm jb_k$. So, mathematically the time-domain equivalent of the reflection coefficient can be expressed as the sum of damped sinusoids.

There are methods to identify the natural frequencies and the complex amplitudes, λ_k and A_k, for which the frequency-domain counterpart of Eq. (4) in partial fraction form,

$$\hat{W}(\omega) = A_0 + \sum_k \frac{A_k}{s - j\lambda_k} + \frac{A_k^*}{s - j\lambda_k^*}, \tag{5}$$

or in rational form,

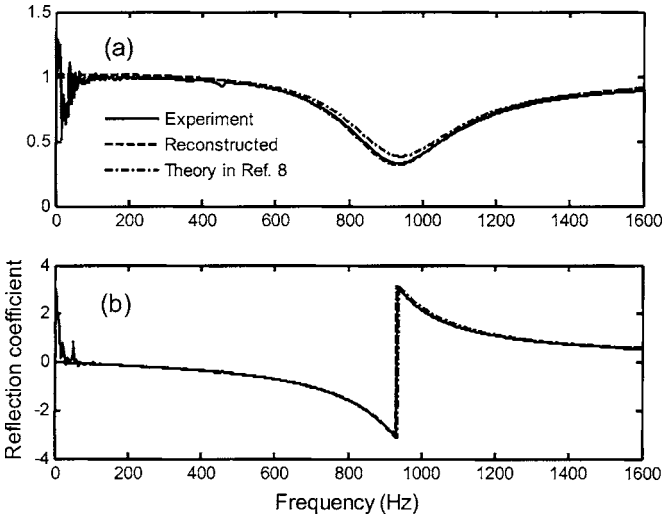

FIG. 1. (a) Magnitude. (b) Phase. Comparison of various presentations of the reflection coefficient for the MPP with hole diameter 1.0 mm, plate thickness 1.0 mm, porosity 1.2% and cavity depth 20 mm.

$$\hat{W}(\omega) = \frac{\sum_{n=0}^{M} p_n s^n}{1 + \sum_{m=1}^{M} q_m s^m}, \tag{6}$$

where $s=j\omega$ and p_n and q_m are real coefficients, would be useful. Given a set of N $(N>2M+1)$ values of $\hat{W}(\omega)$ at the discrete frequencies ω_l, an iterative least-squares approach can be used to compute these coefficients.[7] Then, it is straightforward to factorize Eq. (6) for λ_k and A_k.

III. VALIDATION OF DHO IMPEDANCE CHARACTERIZATION

A. Impedance tube measurement

We first examined several real impedance boundaries formed by practical sound-absorbing materials or structures in a B&K 4206 impedance tube. A single-layer MPP is measured and its reflection coefficient presented in Fig. 1. It is shown from the analysis of the above frequency-domain identification method that the reflection coefficient of the MPP possesses only one pole over the frequency range from 0 to 1600 Hz, so the measured curve can be fairly well reconstructed by the damped-sinusoid pair given in Table I. The theoretical results computed from Maa's[8] formula are also given in Fig. 1 for comparison. It is further shown that

TABLE I. Identified DHOs for the MPP and the porous panel.

Types of sound-absorbing structures	Natural frequencies (Hz), $\lambda_k/2\pi$	Complex amplitudes[a] (Hz), A_0 or $A_k/2\pi$ $(k\geqslant 1)$
Microperforated panel	–	1.0
	$\pm 892.6 + j244.0$	$-321.1 \mp j96.3$
Porous panel	–	−0.2827
	$0.0 + j86.2$	−25.0
	$0.0 + j283.8$	520.0
	$\pm 1265.3 + j741.0$	$500.2 \pm j582.6$

[a]The values of A_0 correspond to the null natural frequency indicted by "-".

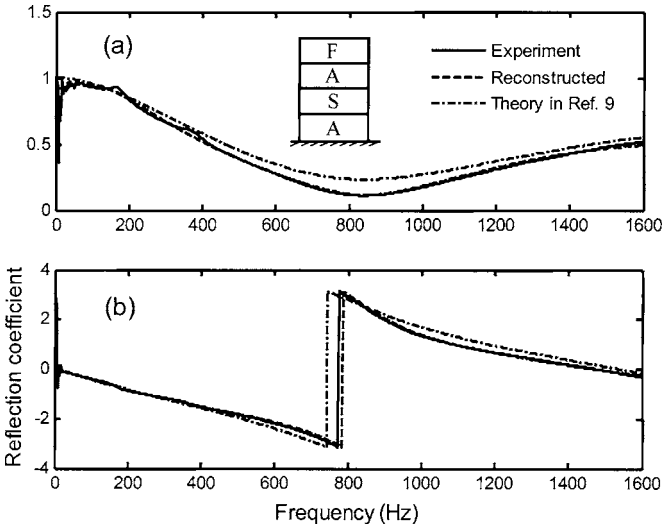

FIG. 2. (a) Magnitude. (b) Phase. Comparison of various presentations of the reflection coefficient for the porous panel of composite layers of FASA (F-fiber, S-sponge, A-air) and respective thicknesses of 28, 27, 25, and 20 mm.

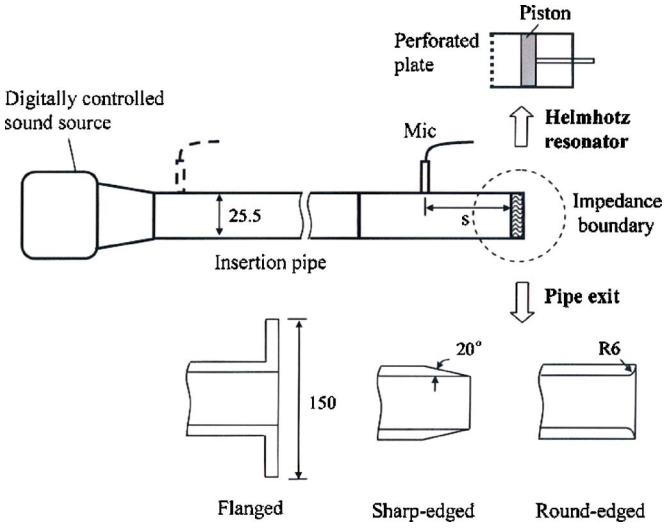

FIG. 3. Schematic of impulse experiment for impedance boundaries of (a) Helmholtz resonator and (b) pipe exit; distance from microphone to impedance sample $s=391$ mm for the Helmholtz resonator and $s=417$ mm for the pipe exit.

the real part of the identified $\lambda_k/2\pi$ is nearly equal to the resonant frequency of the single-layer MPP, 894 Hz, while its imaginary part is related to the damping factor.

Porous panels are also common sound-absorbing structures. A porous panel made of common sound-absorbing materials, a fiber of flow resistivity 7526.8 rayls/m and sponge of 748.0 rayls/m, was examined. The identified natural frequencies λ_k and the complex amplitudes A_k of the porous panel are given in Table I. The measured and the reconstructed reflection coefficients of the porous panel are shown in Fig. 2, and the theoretical results based on Delany and Bazley's[9] one-parameter empirical model are also given for comparison purpose. It is shown that the porous panel behaves in a way similar to the MPP, but more pairs of DHO are needed to reconstruct the measured reflection coefficient. It is evident that the resonant characteristics of the porous panel are more complex than that of the single-layer microperforated panel.

B. Impulse measurement

Figure 3 shows the experimental setup, which mainly consists of a one-dimensional waveguide made of a pipe 25.5 mm in diameter, an impedance terminus at one end of the waveguide and an impulse sound source at the opposite end. A B&K $\frac{1}{4}$-in. microphone, flush mounted into the pipe wall, is used to measure the sound pressure in the duct; the measured signal is digitally sampled by an NI DAQ Board 6062E. The impulse sound source, which is made of a cabinet loudspeaker, can be controlled to emit sound pulses of arbitrary waveform and duration as short as 0.5 ms with high fidelity, as demonstrated in Ref. 10. In order to control the sound emission, it first needs to obtain the transfer function of the sound source connected to an infinite long pipe. For this purpose, a 1.4-m-long insertion pipe is used to increase the time delay between the initial sound pulse and the subsequent reflections from the pipe terminus and thereby edit out the unwanted reflections. The microphone is first positioned near the sound source, indicated by the dashed line in Fig. 3, to obtain the transfer function of the source-pipe system, and then moved to the side of the impedance boundary to measure the sound pulse reflection.

In the experiment, the terminus is physically either a Helmholtz resonator or a pipe exit. As shown in Fig. 3, the Helmholtz resonator is made of a micro-perforated plate backed by a cavity, whose depth can be adjusted by moving the piston. Three different types of pipe exit, flanged, sharp-edged, and round-edged, are investigated in the experiment, among which the sharp-edged one is used to reduce the influence of the pipe wall thickness. The experiment of the Helmholtz resonator surface was carried out at 22 °C ambient temperature and that of the pipe exit at 17 °C.

Acoustic pulses as short as 1 ms are used in the experiment, and they are of three different desired waveforms referred as to sine, three-pole, and Butterworth (Appendix A). Since the incident sound pulse generated at one end of the pipe is much shorter than the time delay corresponding to twice the distance from the microphone to the test sample at the other end, the incident sound pulse can be clearly separated from the reflected pulse. It is thus straightforward to obtain the reflection coefficient of a test sample from the Fourier-transformed time signals per Eq. (1) and its natural frequencies and complex amplitudes by the identification method in Sec. II. In a test, the three-pole sound pulse is used for DHO identification and characterization. For subsequent analyses of various incident pulses $p^+(t)$, the reflected pulses $p^-(t)$ are predicted using the efficient recursive formula of Ref. 4,

$$p_k^-(t) = A_k[p^+(t) + z_k p^+(t-\Delta t)]\frac{\Delta t}{2} + z_k p_k^-(t-\Delta t)$$

$$p^-(t) = A_0 p^+(t) + \sum_k p_k^-(t) \tag{7}$$

where Δt is the time step, and $z_k = \exp(j\lambda_k \Delta t)$ ensures Eq. (7)'s stability for causal reflection, i.e., $|z_k| < 1$ when $\mathrm{Im}\lambda_k$

TABLE II. Identified DHOs for the Helmholtz resonators.

Cavity depth (mm)	Natural frequencies (Hz), $\lambda_k/2\pi$	Complex amplitudes[a] (Hz), A_0 or $A_k/2\pi$ $(k \geqslant 1)$
20	–	0.849
	$\pm 1259.6 + j718.1$	$-623.8 \mp j471.9$
60	–	0.836
	$\pm 502.1 + j569.5$	$-575.5 \mp j707.0$
	$\pm 3098.9 + j149.7$	$-65.3 \mp j110.4$
	$\pm 5904.4 + j127.6$	$-51.6 \mp j60.2$

[a]The values of A_0 correspond to the null natural frequency indicted by "-".

>0. Finally, the time-domain impedance characterization method is validated by the well-matched predicted and measured reflections.

1. Helmholtz resonators

For the Helmholtz resonator with a cavity of 20 mm, the identified natural frequencies and complex amplitudes are given in Table II. Figure 4 shows that the reflection coefficient of the Helmholtz resonator can be well reconstructed with only one damped harmonic oscillator. In Fig. 5, the predicted reflection pulse computed from Eq. (7) is compared with the measured reflection. It is not surprising to find the well-matched pulses, Fig. 5(a), for the three-pole pulse were used to identify the characterizing parameters. The DHO descriptor of an impedance boundary is rather validated by the excellent agreement between the predicted and measured reflection pulses for the sine and Butterworth incident, respectively shown in Figs. 5(b) and 5(c). When the depth of the Helmholtz resonator is increased to 60 mm, three pairs of natural frequencies and complex amplitudes, listed in Table II, are identified and the well-reconstructed reflection coefficient is shown in Fig. 6. It can be seen in Fig. 7 that the predicted and measured reflected pulses agree well not only for the three-pole incident, but also for the sine and the Butterworth pulses. In Figs. 4 and 6, the theoretical reflection coefficients from Ref. 8 are also plotted for comparison.

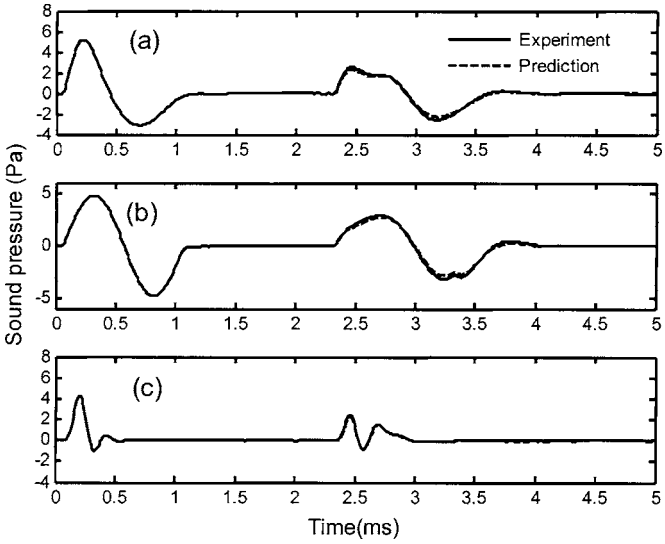

FIG. 5. Comparison of predicted and measured sound pulses reflected from the Helmholtz resonator of Fig. 4 on the (a) three-pole, (b) sine, and (c) Butterworth incident pulse.

As we know, a sound-absorbing structure in resonance has the locally lowest acoustic reflection or highest absorption coefficient. For the 20-mm cavity Helmholtz resonator, the one identified DHO is clearly associated with the minimum of the reflection coefficient and so are the three identified DHOs for the 60-mm cavity Helmholtz resonator. In fact, the real parts of the $\lambda_k/2\pi$ of these DHOs approximate respectively the frequencies where the minima of the reflection coefficient are found with minor differences attributable to the imaginary parts. Therefore, in these and the MPP case in Sec. III A, the association between the identified DHOs and the intrinsic resonances of an impedance boundary is clear.

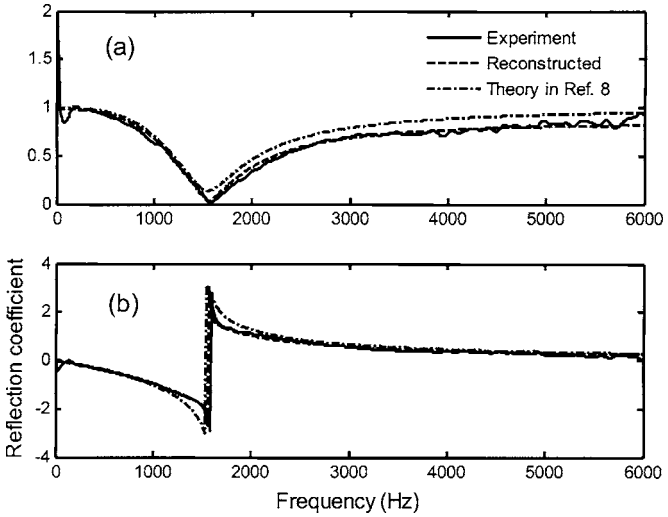

FIG. 4. (a) Magnitude. (b) Phase. Comparison of various presentations of the reflection coefficient for the Helmholtz resonator with hole diameter 0.3 mm, plate thickness 0.15 mm, porosity 0.785%, and cavity depth 20 mm.

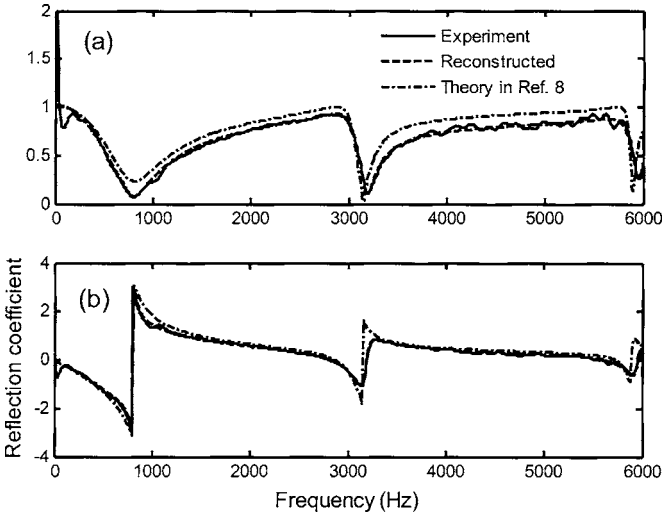

FIG. 6. (a) Magnitude. (b) Phase. Comparison of various presentations of the reflection coefficient for the Helmholtz resonator with hole diameter 0.3 mm, plate thickness 0.15 mm, porosity 0.785%, and cavity depth 60 mm.

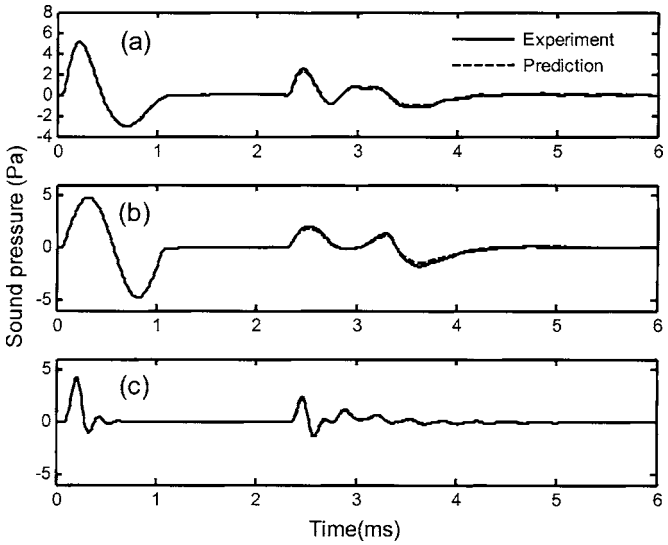

FIG. 7. Comparison of predicted and measured sound pulses reflected from the Helmholtz resonator of Fig. 6 on the (a) three-pole, (b) sine, and (c) Butterworth incident pulse.

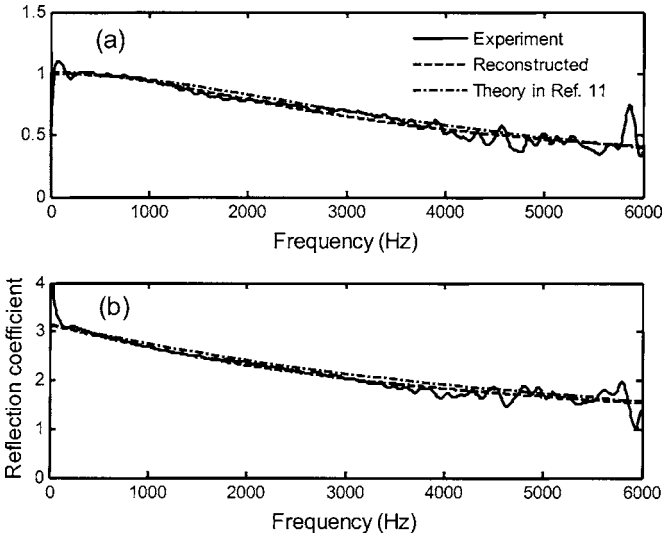

FIG. 8. (a) Magnitude. (b) Phase. Comparison of various presentations of the reflection coefficient for the flanged pipe exit.

2. Pipe exits

As a common acoustic element the pipe exit has long attracted much research attention. The radiation impedance of a circular pipe exit with an infinite flange has been derived by Morse and Ingard[11] and that of the unflanged one by Levine and Schwinger.[12] To the authors' best knowledge, these analytical works have so far no direct experimental confirmation in the open literature. For such open-end measurements the common impedance tube would be inapplicable due to its sensitivity to the external variances particularly at low frequency. The majority of experiments[13–15] are shock tube based, in which the involved flow nonlinearity prevents a direct comparison with the linear theories. Since the present time-domain impulse method has a finite extent in space and time and is not susceptible to external variances as frequency-domain methods, it is hoped that the following results on the pipe exit would complement these classical works.

According to Morse and Ingard,[11] the acoustic impedance of a pipe exit with an infinite flange is given as below,

$$Z(\bar{\omega}) = 1 - \frac{2J_1(\bar{\omega})}{\bar{\omega}} + j\frac{4}{\pi}\int_0^{\pi/2} \sin(\bar{\omega}\cos x)\sin^2 x\, dx, \quad (8)$$

where $\bar{\omega}$ is the angular frequency normalized by the sound speed and the pipe diameter. The reflection coefficient can be computed from Eq. (2). It has been shown in Ref. 5 that the low-frequency approximation of Eq. (8), $Z(\bar{\omega})=\frac{1}{8}\bar{\omega}^2 + j(4/3\pi)\bar{\omega}$, or the high-frequency approximation, $Z(\bar{\omega})=1 + j\pi/4\bar{\omega}$, renders a noncausal reflection coefficient. Nonetheless, it is shown in Appendix B that the exact reflection coefficient given by Eq. (8) is causal and can be cast as an infinite sum of DHOs.

Figure 8 not only shows that the measured reflection coefficient via the three-pole acoustic pulse agrees well with the theory of Morse and Ingard,[11] but also that the measured reflection coefficient of the flanged pipe exit can be well reconstructed with only one damped harmonic oscillator for the frequency range of 0–6000 Hz, or the normalized frequency range of 0–0.45. This result is consistent with the analysis in Appendix B, which gives a purely imaginary predominant pole at $\lambda_1=1.456j$ and residue of $A_1=-1.848$ in comparison with the corresponding measured values of $1.128j$ and -1.359 given in Table III, respectively. The limited frequency range of measurement prevents the identification of the higher-order poles whose normalized natural frequencies are above 7.906, much higher than the cut-on frequency of the higher-order modes in the pipe. The small deviations between the experimentally identified and exact values can be simply due to dropping all higher order poles in the approximation. Figure 9 further demonstrates that the reflected pulses can be very well predicted based on either the DHO of the three-pole incident pulse or when cross-checked with the sine and Butterworth incident pulses. Different from those Helmholtz-resonator impedance surfaces, the DHOs of the pipe exit are purely damped, i.e., no real-valued resonance frequency.

It is shown in Fig. 10 that the sharp-edged pipe exit has similar acoustic properties as those of the flanged one, but its damping factor, i.e., the imaginary part of the natural frequency, is larger than that of the flanged pipe exit (Table III), thus allowing more acoustic energy to reflect back. Also shown in the figure is that the measured and the recon-

TABLE III. Identified DHOs for the pipe exits.

Type of pipe exit	Natural frequencies (Hz), $\lambda_k/2\pi$	Complex amplitudes[a] (Hz), A_0 or $A_k/2\pi$ $(k\geqslant 1)$
Flanged	–	0.181
	$0.0+j2453.8$	−2918.7
Sharp-edged	–	0.232
	$0.0+j3209.7$	−4001.7
Round-edged	–	0.10
	$0.0+j2576.4$	−2946.6

[a]The values of A_0 correspond to the null natural frequency indicted by "-".

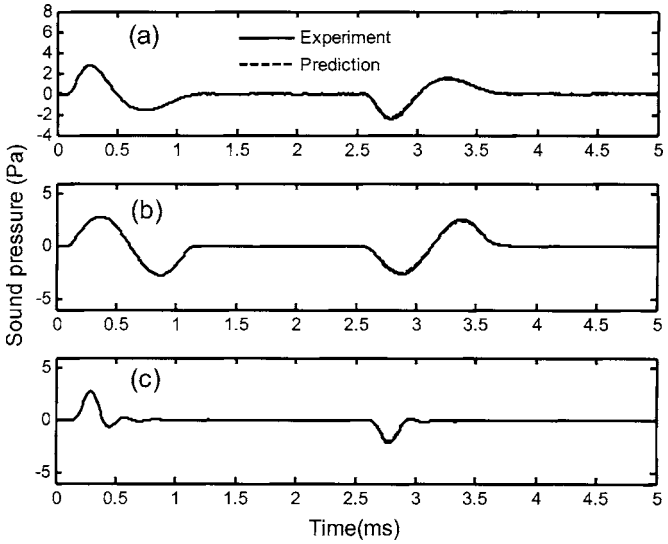

FIG. 9. Comparison of predicted and measured sound pulses reflected from the pipe exit of Fig. 8 on the (a) three-pole pulse, (b) sine pulse, and (c) Butterworth incident pulse.

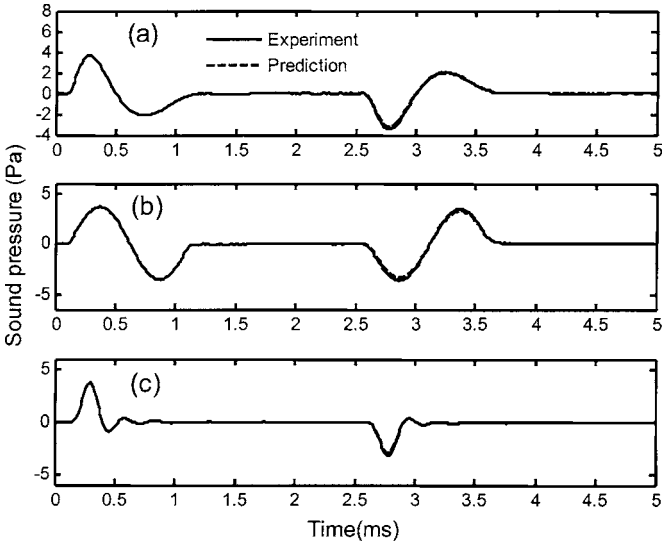

FIG. 11. Comparison of predicted and measured sound pulses reflected from the pipe exit of Fig. 10 on the (a) three-pole pulse, (b) sine pulse, and (c) Butterworth incident pulse.

structed reflection coefficient agree well with the theory of Levine and Schwinger[12] for the circular pipe exit of zero wall thickness. Figure 11 shows the result for the pulse reflection at the sharp-edged pipe exit. In Figs. 12 and 13 it is demonstrated that the acoustic properties of a round-edged pipe exit can also be well represented by a purely damped harmonic oscillator, for which no analytical solution is known to the authors. From the identified DHO descriptor given in Table III, we can see that the acoustic properties of the round-edged pipe exit are quite close to those of the flanged one.

In terms of the DHO description of its acoustic properties, we can conclude that a pipe exit, unlike a Helmholtz resonator, is basically a nonresonant acoustic element at least in the case below the cutoff frequency.

IV. CONCLUSIONS

We have shown here that common sound-absorbing materials and structures possess the characteristics of composite DHO, which is a simpler and physically more meaningful descriptor than the conventional impedance in the following ways:

(1) Within the frequency range of practical interest, the reflection coefficient of an impedance boundary can be well represented by the sum of only a few DHOs, bearing the intrinsic resonant characteristics as the natural frequencies of the Helmoltz resonator structures or the nonresonant pure dampings of pipe exits. Unlike the conventional frequency-domain characterization and measurement of impedance, such as in an impedance tube, the DHO descriptor gives a reliable extended broadband description to the lowest frequencies where the classically measured impedance data are often unreliable due to sensitivity to error.
(2) This has been validated by the good agreement between

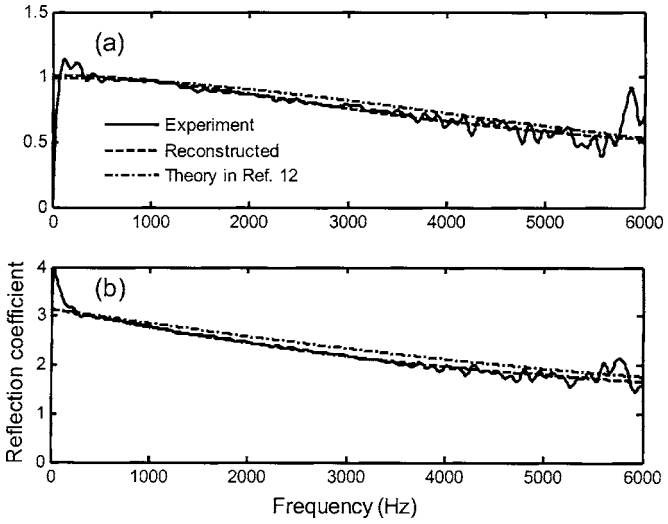

FIG. 10. (a) Magnitude. (b) Phase. Comparison of various presentations of the reflection coefficient for the sharp-edged pipe exit.

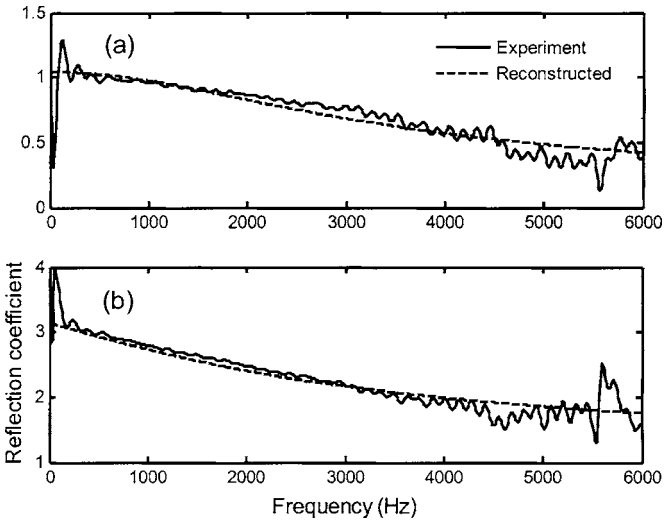

FIG. 12. (a) Magnitude. (b) Phase. Comparison of various presentations of the reflection coefficient for the round-edged pipe exit.

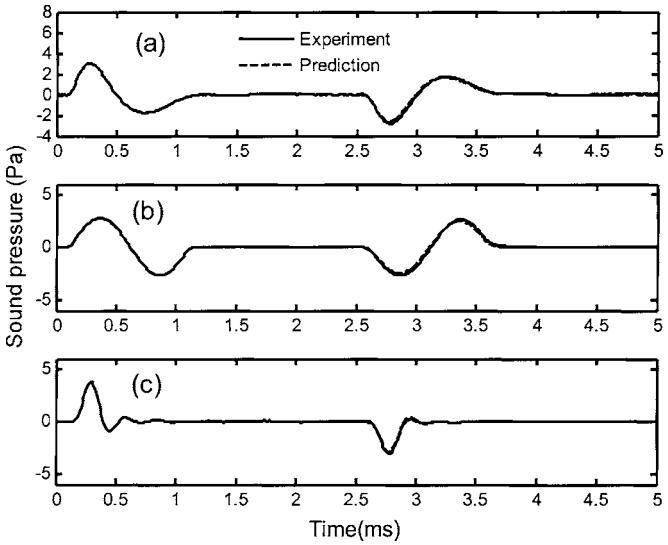

FIG. 13. Comparison of predicted and measured sound pulses reflected from the pipe exit of Fig. 12 on the (a) three-pole pulse, (b) sine pulse, and (c) Butterworth incident pulse.

measured and predicted pulses in the time- and frequency-domain and by various theories on a one-dimensional waveguide.

(3) We have yet encountered, so far, in our identification of DHOs of impedance boundaries, from either the measured pulses or the exact analytical solution of the reflection coefficient, a non-causal result.

(4) A set of causal DHOs is readily employed as a stable TDIBC for CAA.

Therefore, it is physically sound and numerically advantageous to characterize an impedance surface as a sum of DHOs.

ACKNOWLEDGMENTS

Financial support for the second author on the Hong Kong Research Grants Council's Competitive Earmarked Research Grant PolyU UGC earmarked Grant 5158/01E is gratefully acknowledged.

APPENDIX A: DESIRED WAVEFORMS OF THE SOUND PULSE IN EXPERIMENT

The three desired waveforms are described in detail as follows. The sine pulse is the simplest one and consists of a single-period sine wave. The three-pole pulse is synthesized from three pairs of damped sinusoids as below,

$$p(t) = H(t)\sum_{k=1}^{3} A_k \exp(j\lambda_k t) + A_k^* \exp(j\lambda_k^* t), \tag{A1}$$

where λ_k, $\lambda_k^* = \pm 2598.7 + j4394.7$, $\pm 7462.2 + j4223.7$, $\pm 13456.2 + j2635.4$ and correspondingly A_k, $A_k^* = 1.2002 \pm j2.6113$, $-1.2277 \mp j1.2012$, $0.027468 \mp j0.102788$. The Butterworth pulse is the impulse response of a sixth-order Butterworth low-pass filter whose cutoff frequency is 5 kHz. The duration of all the pulses is approximately 1 ms.

APPENDIX B: CAUSALITY OF THE REFLECTION COEFFICIENT OF FLANGED PIPE EXIT

Following Rudinger's[13] analysis, the first-order Bessel function is written in the following integral form:

$$J_1(\bar{\omega}) = \frac{2\bar{\omega}}{\pi}\int_0^{\pi/2} \cos(\bar{\omega}\cos x)\sin^2 x\, dx. \tag{B1}$$

The poles of $\bar{W}(\omega)$, $\lambda_k, \lambda_k^* = \pm\alpha_k + j\beta_k$, satisfy the relation

$$1 + Z(\bar{\omega}) = 0. \tag{B2}$$

Substituting Eqs. (8) and (B1) into the above equation, we get

$$\int_0^{\pi/2} e^{\beta_k \cos x} \cos(\alpha_k \cos x)\sin^2 x\, dx = \frac{\pi}{2} \tag{B3}$$

and

$$\int_0^{\pi/2} e^{\beta_k \cos x} \sin(\alpha_k \cos x)\sin^2 x\, dx = 0.$$

Assuming $\beta_k \leqslant 0$, we have $e^{\beta_k \cos x} \leqslant 1$ since $0 \leqslant x \leqslant \pi/2$. Thus, the following inequalities hold:

$$\left|\int_0^{\pi/2} e^{\beta_k \cos x} \cos(\alpha_k \cos x)\sin^2 x\, dx\right| \leqslant \int_0^{\pi/2} |\cos(\alpha_k \cos x)|\sin^2 x\, dx \leqslant \int_0^{\pi/2} \sin^2 x\, dx = \frac{\pi}{4}. \tag{B4}$$

The contradiction between Eqs. (B3) and (B4) indicates that all the poles of $W(\omega)$ must lie in the upper half of the complex ω plane, thus confirming the causality of Morse and Ingard's[11] analytical solution for the flanged pipe opening.

Equation (8) provides a direct means for solving Eq. (B2) for the poles of the reflection coefficient. Numerically, a Newton-Raphson search gives the first three pairs of normalized poles and residues at $\bar{\lambda}_k, \bar{\lambda}_k^* = 1.456j$, $\pm 7.906 + 3.510j$, $\pm 14.42 + 4.312j$ and $\bar{A}_k, \bar{A}_k^* = -1.848, -1.0 \pm 0j$, $-1.0 \pm 0j$.

[1] C. K. W. Tam and L. Auriault, "Time-domain impedance boundary conditions for computational acoustics," AIAA J. **34**(5), 917–923 (1996).
[2] Y. Ozyoruk, L. N. Long, and M. G. Jones, "Time-domain numerical simulation of a flow-impedance tube," J. Comput. Phys. **146**(1), 29–57 (1998).
[3] Y. H. Berthelot, "Surface acoustic impedance and causality," J. Acoust. Soc. Am. **109**(4), 1736–1739 (2001).
[4] K.-Y. Fung and H. Ju, "Broadband time-domain impedance models," AIAA J. **39**(8), 1449–1454 (2001).
[5] H. Ju and K.-Y. Fung, "Time-domain impedance boundary conditions with mean flow effects," AIAA J. **39**(9), 1683–1690 (2001).
[6] L. B. Felsen, *Transient Electromagnetic Fields* (Springer-Verlag, Berlin, 1976).
[7] K. Sanathanan and J. Koerner, "Transfer function synthesis as a ratio of two complex polynomials," IEEE Trans. Autom. Control **8**, 56–58 (1963).
[8] D. Y. Maa, "Microperforated-panel wideband absorbers," Noise Control Eng. J. **29**(3), 77–84 (1987).
[9] M. E. Delany and E. N. Bazley, "Acoustical properties of fibrous absorbent materials," Appl. Acoust. **3**, 105–116 (1970).
[10] X. Jing and K.-Y. Fung, "Generation of desired sound impulses," J. Sound Vib. (to be publsihed).

[11]P. M. Morse and K. U. Ingard, *Theoretical Acoustics* (McGraw-Hill, New York, 1968).
[12]H. Levine and J. Schwinger, "On the radiation of sound from an unflanged circular pipe," Phys. Rev. **73**(4), 383–406 (1948).
[13]G. Rudinger, "On the reflection of shock waves from an open end of a duct," J. Appl. Phys. **26**(8), 981–993 (1955).
[14]J. Brown and A. Vardy, "Reflection of pressure waves at tunnel portal," J. Sound Vib. **173**(1), 95–111 (1994).
[15]H. D. Kim and T. Setoguchi, "Study of the discharge of weak shocks from an open end of a duct," J. Sound Vib. **226**(5), 1011–1028 (1999).